*J. Astrophys. Astr.* (2018) 39:19
https://doi.org/10.1007/s12036-017-9509-y



# Spectral properties of the accretion discs around rotating black holes

SAMIR MANDAL[1,*] and SOUMEN MONDAL[2]

[1] Indian Institute of Space Science and Technology, Thiruvananthapuram 695 547, India.
[2]Department of Physics, Jadavpur University, Kolkata 700 032, India.
*Corresponding author. E-mail: samir@iist.ac.in

MS received 11 September 2017; accepted 25 December 2017; published online 10 February 2018

**Abstract.** We study the radiation properties of an accretion disc around a rotating black hole. We solve the hydrodynamic equations and calculate the transonic solutions of accretion disc in the presence of shocks. Then we use these solutions to generate the radiation spectrum in the presence of radiative heating and cooling processes. We present the effect of spin parameter of the black hole on the emitted radiation spectrum. In addition, attention has also been paid to the variation in energy spectral index with Kerr parameter and accretion rate. We find that spectral index becomes harder as the spin parameter changes from negative (accretion disc is counter-rotating with respect to the black hole spin) to a positive value. Finally, we compute and compare the spectral characteristics due to a free-fall flow and a transonic flow. We notice significant differences in high energy contributions from these two solutions.

**Keywords.** Accretion disc—radiation spectrum—rotating black hole.

## 1. Introduction

Accretion onto a black hole (BH) is one of the important processes to study the physics under strong gravity. Bondi (1952) studied spherical accretion of matter in Newtonian gravity but a free-fall flow is radiatively inefficient due to high infall velocity. Shakura and Sunyaev (1973) assumed a Keplerian angular momentum distribution of matter in Newtonian gravity and studied the structure of the so-called standard accretion disc. This work has been extended to general relativity by Novikov & Thorne (1973) and Page & Thorne (1974). The standard disc is radiatively efficient and the observed luminosity in ultraviolet range for active galactic nuclei (Sun & Malkan 1989) as well as soft X-ray emission from galactic compact binary systems could be explained (Belloni *et al.* 2005; Remillard & McClintock 2006). But a standard Keplerian disc is not able to address the high energy X-ray/gamma ray radiation observed in galactic/extra-galactic BH systems. Also the observations related to high-frequency quasi-periodic oscillations (Belloni *et al.* 2001; Strohmayer 2001), asymmetric broadening of Fe $K_\alpha$ line (Reeves *et al.* 2006; Patrick *et al.* 2012), high energy emissions extended to MeV (Chakrabarti & Mandal 2006; Sabatini *et al.* 2013), relativistic jets (Jorstad & Marscher 2004; Mirabel & Rodríguez 1999) indicate that the associated systems may be harbouring rotating BHs.

Over the past few decades, several notable works on accretion disc models (Lightman & Eardley 1974; Ichimaru 1977; Galeev *et al.* 1979; Rees *et al.* 1982; Muchotrzeb & Paczyński 1982; Chakrabarti & Titarchuk 1995; Narayan & Yi 1995; Abramowicz *et al.* 1995) were proposed to address these issues. But these previous works are mostly focussed either on the detail hydrodynamics of the flow without including various radiative processes or based on radiative properties of the accretion disc excluding rigorous hydrodynamics of the flow. Hence, a self-consistent hydrodynamical study in Kerr geometry in the presence of radiative processes is required and the results from hydrodynamical study to understand the radiative properties of the accretion disc should be used. This can be done either through numerical simulations or analytical studies.

An analytical study of accretion flow, under a general relativistic prescription of Kerr geometry, in the presence of heating and cooling processes is extremely difficult and has not yet been attempted properly. Rather several attempts (Chakrabarti & Khanna 1992; Artemova *et al.* 1996; Semerák & Karas 1999; Mukhopadhyay 2002; Ivanov & Prodanov 2005; Chakrabarti & Mondal 2006) have been made to develop an effective

potential which can mimic all the essential properties of Kerr geometry. The advantage of such a pseudo-Kerr potential is that it provides a Newtonian analogue of Kerr geometry and hence dealing hydrodynamics in the presence of radiative processes becomes much easier. In parallel, several groups (Hawley & Villiers 2004; Fragile *et al.* 2007; Sądowski *et al.* 2014, 2015) approached the problem using time-dependent general relativistic magneto-hydrodynamic simulation (GRMHD). Recently Sądowski *et al.* (2017) and Narayan *et al.* (2017) calculated the radiation spectrum from a two-temperature accretion disc for a range of accretion rates using GRMHD simulation with a realistic prescription of hydrodynamics and radiative processes.

Previous analytical studies of radiation properties (Cunningham 1975; Luminet 1979; Hanawa 1989; Ebisawa & Mitsuda 1991; Bao *et al.* 1994; Li *et al.* 2005) of accretion disc around a Kerr BH are based on standard Keplerian accretion disc where the source of radiation is the multicolour black body photons. Whereas observation results (Smith *et al.* 2001, 2002; Nandi *et al.* 2012; Iyer *et al.* 2015) show that the presence of a sub-Keplerian matter in the accretion flow is very important to understand the spectro-temporal behaviour of the emitted radiation from accretion disc. This indicates that a general accretion disc must be two components including both Keplerian and sub-Keplerian flow of matter.

In this paper, we aim to study mainly the radiation properties of a two-component accretion disc around a rotating black hole where BH geometry is described by a pseudo-Kerr (PK) potential (Chakrabarti & Mondal 2006). We use the transonic hydrodynamic flow solutions in the presence of shock to calculate the radiation spectrum from a sub-Keplerian disc. We specifically choose the shock solutions as the dense and hot post-shock region regulates the high energy part of the radiation spectrum. Also we study the effect of BH spin on the radiation spectrum. We present basic hydrodynamics and solution procedure in the next section. In section 3, we present the results of our calculations and discuss the physical importance of these results. Finally, in section 4, we give a summary of this work.

## 2. Model description and solution procedure

In general, the accretion flow around a BH is known to have predominantly two components (Chakrabarti & Titarchuk 1995): an optically thick and geometrically thin Keplerian accretion disc (hereafter KD) lies on the equatorial plane and an optically thin sub-Keplerian flow (hereafter SKD) sandwiches the KD from top and bottom. BH does not have any hard surface but in the presence of angular momentum in the SKD, the centrifugal force becomes important close to the central object. The centrifugal force slows down the matter inflow, allowing a piling up of matter or discontinuous shock transition close to the BH. Hence, the central part of the accretion disc becomes dense and hot due to compression and conversion of bulk kinetic energy into thermal energy. This hot central region acts as an effective boundary around the black hole. For presentation purpose, a sub-Keplerian disc (SKD) can be be divide into a pre-shock region (hereafter PRSR) and a post-shock region (hereafter POSR). We assume that the KD truncates at the shock location (Giri & Chakrabarti 2013) because a cold Keplerian disc may not survive in the hot POSR. KD produces multi-colour black body photons and a fraction of these soft photons from the KD is inverse Comptonized (Sunyaev & Titarchuk 1980, 1985) by hot electrons in POSR. Hence, POSR is responsible for producing high-energy radiations from the accretion disc. Here we are going to study the properties of these high energy radiations from a two-temperature (Narayan & Yi 1995; Chakrabarti & Titarchuk 1995) and two-component flow. The accretion disc is axisymmetric and the flow is in vertical equilibrium (Chakrabarti 1989). Here, we consider KD is static and the dynamics of SKD determines the accretion disc radiation properties. The radial distance ($x$), flow velocity ($u$) and specific angular momentum ($\lambda$) are measured in units of $r_g = GM/c^2$, $c$ and $GM/c$ respectively, where $G$ is the gravitational constant, $M$ is the mass of the black hole expressed in solar mass ($M_\odot$) and $c$ is the speed of light. The mass accretion rate ($\dot{m}$) is expressed in units of Eddington accretion rate.

### 2.1 *Basic hydrodynamic equations*

The hydrodynamic description of an accretion disc is given by three basis governing equations, namely, the Euler equation, the continuity equation and the entropy generation equation (or equation of state). In the absence of dissipation in the flow, the above equations conserve the specific energy, specific angular momentum and the mass flux. The conserved quantities of the flow along with the equation of state entirely governs the hydrodynamic features of the accretion disc.

($a$) *Energy conservation equation*:

The conserved specific energy ($\mathcal{E}$) in PK geometry is given by

$$\mathcal{E} = \frac{1}{2}u^2 + \frac{\gamma}{\gamma - 1}\frac{P}{\rho} + \Phi_{\rm eff}, \tag{1}$$

where $\gamma$, $P$ and $\rho$ are the adiabatic index, isotropic pressure and mass density of the flow respectively. The different terms in equation (1) are the specific kinetic energy, the specific enthalpy, and the potential energy of the flow respectively. The effective potential, $\Phi_{\rm eff}$ (Chakrabarti & Mondal 2006) is given in spherical polar coordinate as

$$\Phi_{\rm eff}(r,\theta) = 1 - \frac{1}{r - r_0} + \frac{2a(\tilde{l} + \omega r^2)}{r^3 \sin\theta} + \frac{\alpha^2(\tilde{l} + \omega r^2)^2}{2r^2 \sin^2\theta},$$

where $a$ is the Kerr parameter, i.e., angular momentum per unit mass of BH, $r_0$ is a constant factor depending on $a$, $\alpha$ is the redshift factor, $\tilde{l}$ is the specific angular momentum of the particle and $\omega$ is the frame dragging term (for details on expression of these terms, see Chakrabarti & Mondal 2006). The potential denotes a combination of gravitation potential energy (second term) and centrifugal potential energy (last term). Note that the third term in the expression is related to spin orbit coupling which represents the rotational features of the spacetime in Kerr geometry. In an axisymmetric disc, the radial distance $x = r\sin\theta$, where $(r,\ \theta)$ are the spherical polar coordinates. Using this pseudo-Kerr potential, $\Phi_{\rm eff}$, a complete particle dynamics (Chakrabarti & Mondal 2006) and hydrodynamic properties (Mondal & Chakrabarti 2006) of an adiabatic flow have been studied in detail. In comparison to the general relativistic results, the errors in this Newtonian formalism are found to be very small and even less than 1 per cent in most of the cases ($-1 \le a < 0.8$). Here a negative value of $a$ implies an accretion disc which is counter-rotating with respect to the direction of the BH spin. Also this potential can well mimic both the Kerr and Schwarzschild spacetime by changing the Kerr parameter, $a$, only.

(*b*) *Mass conservation equation*:

In the present study, we consider a radial flow in which vertical component of the flow velocity is negligible. Considering Euler equation in the vertical direction yields vertical components of the pressure gradient force which is necessarily equal to the vertical component of the gravitational force. Balancing the two forces, we obtain vertical height of the disc as

$$h(x) = c_{\rm s} x^{1/2}\left(\frac{\partial\Phi_{\rm eff}}{\partial r}\right)^{-1/2}_{\theta=\pi/2}, \tag{2}$$

where $c_{\rm s}$ is the local sound speed and is related to pressure as $c_{\rm s}^2 = \gamma P/\rho$. Now using $h(x)$, one can easily obtain the mass flux rate at a particular radial distance as

$$\dot{m} = -2\pi\ \rho\, u\, x\, h(x). \tag{3}$$

(*c*) *Entropy generation equations*:

From equations (1) and (3), one easily finds that the total number of unknowns are three, namely: $u$, $P$, $\rho$ with two equations. Therefore, one more equation is required, connecting a relation between $P$ and $\rho$ to solve the equations. The entropy generation equation therefore serves this purpose:

$$\frac{u}{\gamma - 1}\left(\frac{{\rm d}P}{{\rm d}x} - \frac{\gamma P}{\rho}\frac{{\rm d}\rho}{{\rm d}x}\right) = \Lambda - \Gamma, \tag{4}$$

where $\Lambda$ and $\Gamma$ are the cooling and heating terms. In the absence of these terms in the flow, the integration of the above equation yields the adiabatic equation of state $P = K\rho^\gamma$, where $K$ is a constant. We first solve the hydrodynamic equations taking adiabatic equation of state and then introduce the dissipation processes through equation (4). Hence the flow does not remain adiabatic in our study. We iteratively update the flow solutions while solving the entropy generation equation in the presence of different heating/cooling processes. We have described this in detail in section 2.5.

### 2.2 *Transonic nature of the flow*

The specific angular momentum ($\lambda$) of the flow is constant for an adiabatic flow. So, the radial dependancy of the flow variables ($u$, $c_{\rm s}$) can be found by taking derivative of equations (1) and (3) with respect to $x$ and using the adiabatic equation of state. Eliminating $\left(\frac{{\rm d}c_s}{{\rm d}x}\right)$ from the resulting equations, the gradient of the flow velocity can be written as (Mondal & Chakrabarti 2006)

$$\frac{{\rm d}u}{{\rm d}x} = \frac{\left(\frac{2c_{\rm s}^2}{\gamma+1}\right)\left(\frac{h'}{h}\right) - \Phi'_{\rm eff}}{u - \left(\frac{2}{\gamma+1}\right)\left(\frac{c_{\rm s}^2}{u}\right)} = \frac{N}{D}, \tag{5}$$

where a prime denotes derivatives with respect to $x$. The accretion onto a BH is transonic in nature, i.e., flow velocity far away from the BH is subsonic and matter at the horizon must be supersonic (Chakrabarti 1990). Hence, accreting matter must pass through a sonic point and the flow variables must be finite throughout. From equation (5), at the critical point where the denominator ($D$) vanishes, the numerator ($N$) must also disappear to

keep the flow continuous. One can find the sonic point conditions by equating both $N$ and $D$ equal to zero at the critical point. This allows to uniquely determine the flow variables at the sonic point. In order to get a complete solution, we need to know $\left(\frac{du}{dx}\right)_c$, which has a (0/0) form, and here subscript 'c' denotes the sonic point. We use the L'Hospital's rule to calculate the velocity gradient (see equations (15)–(18) of Mondal & Chakrabarti (2006)) at the sonic point. The value of $\left(\frac{du}{dx}\right)_c$ always comes in pairs: real values with opposite sign (saddle type) or imaginary values ('O' type). A real negative value of $\left(\frac{du}{dx}\right)_c$ corresponds to an accretion solution whereas a real positive value corresponds to a wind solution. We then calculate the complete transonic solution (see Chakrabarti 1989; Das 2007 for details) by integrating equation (5) from the sonic point (using flow variables and velocity gradient values at the sonic point) once outward till the outer boundary as well as inward till the BH horizon.

### 2.3 *Shock in accretion*

In a transonic flow, the sonic point characteristics (Fukue 1987; Chakrabarti 1989) show that the accretion flow can have one or more saddle type sonic points. If the flow has only one saddle type sonic point, a subsonic flow at the outer boundary becomes supersonic after passing through the sonic point and enters into the BH supersonically. Flow with two saddle type sonic points, the one close to the horizon is called the inner sonic point and other one is called the outer sonic point. In this case, flow passing through both the sonic points are perfectly acceptable transonic solutions as well. But the flow passing through the outer sonic point has lower entropy than the one passing through the inner sonic point and hence these two solutions can be combined (Zeldovich & Raizer 1968) through a shock transition governed by the shock conditions. For an adiabatic shock transition, this is determined by Rankine–Hugoniot conditions:

(i) energy flux: $\mathcal{E}_+ = \mathcal{E}_-$
(ii) mass flux: $\dot{m}_+ = \dot{m}_-$
(iii) pressure balance: $W_+ + \Sigma_+ u_+^2 = W_- + \Sigma_- u_-^2$,

where '+' and '−' represent the quantities evaluated immediately after and before the shock transition ($x_s$) respectively. As the flow is in vertical equilibrium, we denote the vertically averaged pressure ($W$) and density ($\Sigma$) as

$$W = \int_{-h}^{h} P \, dz = 2 I_{n+1} P_0 h$$

and

$$\Sigma = \int_{-h}^{h} \rho \, dz = 2 I_n \rho_0 h,$$

where $I_n = (2^n n!)^2/(2n+1)!$ (Matsumoto *et al.* 1984) and the polytropic index $n = 1/(\gamma - 1)$. Here $P_0$ and $\rho_0$ denote respectively the pressure and density of the flow at the equatorial plane of the accretion disc. Transonic flow with multiple sonic points does not guarantee a shock transition. It occurs if the above three conditions are satisfied in between two sonic points. In the presence of shock, the flow from the outer boundary first cross the outer sonic point followed by a shock transition and finally enter into the horizon of the BH through the inner sonic point. The shock conditions ensure that the post-shock flow (POSR) contains higher entropy and hence this hot and dense flow controls the high energy spectral characteristic of the accretion disc. In our present study, we concentrate only on the shock solutions. We choose the input parameters ($\mathcal{E}$, $\lambda$) such that the flow has two saddle type sonic points. Then we calculate two separate transonic solutions, one passing through the outer sonic point and the other one passing through the inner sonic point. These two solutions join together at $x_s$ where they satisfy the Rankine–Hugoniot conditions.

### 2.4 *Features of a two temperature flow*

We intend to study the radiation properties of accretion disc and hence the flow includes radiative processes. In general, the accreting plasma around compact objects are ionized and the heating/cooling processes for electrons ($e$) and ions ($i$) are drastically different due to difference in their rest masses. Hence, electrons and protons can have very different temperatures depending on the Coulomb coupling time scale between these two species and the infall time scale of the flow. Using $P = \frac{\rho k_B T_{i,e}}{\mu_{i,e} m_i}$ and taking radial derivative of equation (3), we can rewrite equation (4) separately for ions ($i$) and electrons ($e$) as

$$\frac{dT_i}{dx} = (\gamma_i - 1)\left[\frac{m_i \mu_i}{k_B u \rho}\Lambda_i - T_i\left(\frac{1}{x} + \frac{1}{h}\frac{dh}{dx} + \frac{1}{u}\frac{du}{dx}\right)\right], \tag{6}$$

and

$$\frac{dT_e}{dx} = (\gamma_e - 1)\left[\frac{m_{rmi} \mu_e}{k_B u \rho}(\Lambda_e - \Gamma_e) - T_e\left(\frac{1}{x} + \frac{1}{h}\frac{dh}{dx} + \frac{1}{u}\frac{du}{dx}\right)\right], \tag{7}$$

where $\Lambda_{i,e}$ is the cooling rate for ions and electrons respectively, whereas $\Gamma_e$ is the electron heating rate and we do not include any heating process for ions as the flow is inviscid. Here, $k_B$ is the Boltzmann constant, $m_i$ is the mass of ion, $\gamma_{i,e}$ and $\mu_{i,e}$ are the ratio of specific heats, mean molecular weights for ions and electrons respectively. The ratio of specific heats for ions is taken to be $\gamma_i = 3/2$, whereas the same for electrons is $\gamma_e = 4/3$ as the electrons may possibly be relativistic. We take $\mu_i = 1.23$ and $\mu_e = 1.14$ (Narayan & Yi 1995) for our calculations. We assume that the electrons and ions are coupled through Coulomb coupling ($Q_{ei}$). Since the energy is transferred from the ions to electrons, i.e., $Q_{ei}$ is a cooling term for ions but heating process for electrons. So, the total electron heating is

$$\Gamma_e = Q_{ei}. \tag{8}$$

Ions can cool through inverse bremsstrahlung ($\Lambda_{ib}$) as well along with Coulomb coupling and therefore, the total cooling term for ions is

$$\Lambda_i = Q_{ei} + \Lambda_{ib}. \tag{9}$$

The efficient cooling processes of relativistic electrons include bremsstrahlung ($\Lambda_b$), synchrotron ($\Lambda_s$) and inverse-Comptonization ($\Lambda_{ic}$) processes. Thus, the total electron cooling is given as

$$\Lambda_e = \Lambda_b + \Lambda_s + \Lambda_{ic}. \tag{10}$$

The explicit expressions of all the heating and cooling terms in equations (8)–(10) are presented in Colpi *et al.* (1984), Narayan & Yi (1995) and Mandal & Chakrabarti (2005). For a detailed summary, see equations (7)–(27) of Mandal and Chakrabarti (2005) as we will not be repeating the same expressions here. We assume a stochastic magnetic field ($B_m$) to calculate the synchrotron contribution. The magnetic field strength is estimated from gas pressure as $B_m^2/8\pi = \beta P$, where $\beta$ is a constant. We have taken $\beta = 0.1$ in our study. In general, the inverse-Compton contribution can be written as

$$\Lambda_{ic} = Q_{soft}\mathcal{F}, \tag{11}$$

where $Q_{soft}$ represents the soft photon volume emissivity and $\mathcal{F}$ is a dimensionless enhancement factor associate with the distribution of Comptonizing electrons. Inverse-Comptonization is important only in the POSR due to high density and temperature. In the presence of shock, a fraction of electrons can accelerate across the shock due to Fermi acceleration (Bell 1978a, b) and hence the electron distribution in POSR is a combination of thermal and non-thermal distribution (Mandal & Chakrabarti 2005). The soft photon sources $Q_{soft}$ considered here are photons due to bremsstrahlung, synchrotron photons from thermal and non-thermal electrons in the SKD and multi-colour black body photons from the KD. The factor $\mathcal{F}$ for thermal electrons is taken from Dermer *et al.* (1991) and Mandal & Chakrabarti (2005), whereas the same for non-thermal electrons is given in Rybicki & Lightman (1979) and Mandal & Chakrabarti (2005). The enhancement factor for Comptonization of black-body photons is presented in Chakrabarti & Titarchuk (1995).

Finally, in our spectrum calculation process the major input parameters are $\mathcal{E}$, $\lambda$, $M$ and the two accretion rates $\dot{m}_d$ for KD and $\dot{m}_h$ for SKD respectively.

### 2.5 *Solution procedure*

Chakrabarti and Mandal (2006) calculated the radiation spectra from an accretion disc around a BH using the same radiative cooling processes (equations (8)–(11)) discussed here. But they did not solve the hydrodynamic equations, rather considered a free-fall flow. Also the study was confined around a stationary BH. Here, we intend to see the effect of Kerr parameter on the radiation spectrum as well as the changes in the spectrum if a free-fall flow is replaced by a transonic flow in the presence of shocks. A self-consistent transonic flow solution requires a simultaneous solution of equations (3), (5), (6), (7) for a given set of input parameters. In the presence of heating and cooling, in particular, in the presence of Compton cooling, the analytical form of equation (5) becomes difficult to manage and hence we adopt an iterative method to generate the flow solution. For a given set of input parameters $\mathcal{E}$, $\lambda$ and $a$, we first find the exact transonic shock solution for an inviscid adiabatic flows from equations (1), (3), (5) and using the shock condition (section 2.4). This solution provides the flow velocity profile, $u(x)$, sound speed, $c_s(x)$ (or adiabatic ion temperature), flow density, $\rho(x)$, vertical height, $h(x)$, shock location ($x_s$) and shock compression ratio ($R$). It is a single temperature solution and serves as our initial solution. Now we can solve the entropy equations for ions and electrons [equations (6) and (7)] simultaneously using the initial solution with an electron temperature at the outer boundary $T_{e,out} = \sqrt{m_e/m_i}T_{i,out}$ (Chattopadhyay & Chakrabarti 2002), where $T_{i,out}$ is the ion temperature at the outer boundary and $m_{i,e}$ are their respective masses. In the first iteration, we update $\rho(x)$ and $h(x)$ from equations (2), (3) using the updated ion temperature, keeping the velocity profile same and again solve equations (6) and (7). In the second iteration we do update $u(x)$ and

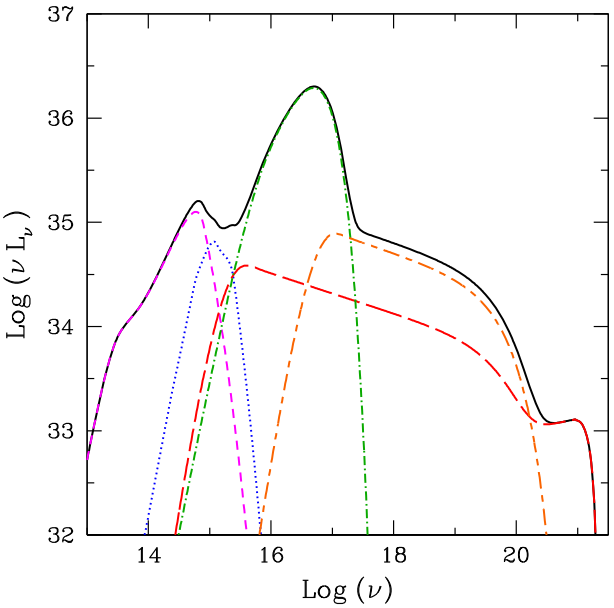


**Figure 1.** The radiation spectrum from an accretion disc around a Kerr black hole. The figure has been drawn for Kerr parameters $a = 0.6$, $\dot{m}_h = 0.3$, $\dot{m}_d = 0.5$, $\mathcal{E} = 1.005$, $\lambda = 2.96$ respectively. For detailed discussions, see text.

$h(x)$ from equations (2), (3) keeping the density profile same as the first iteration. Thus we continue this iterative method until the value of all the flow variables converge. In this iterative method, we keep $x_s$ and $R$ fixed. We then calculate the local radiation emissivity from individual annuli of the disc using these flow variables ($\rho(x)$, $T_e(x)$, $T_i(x)$, $B_m(x)$) for different radiation processes mentioned in section 2.4 and add these local contributions to find the overall spectrum for different radiative processes.

## 3. Results and discussion

We study the radiation properties of a two-temperature and two-component advective disc in pseudo-Kerr geometry around a $10M_\odot$ black hole. We consider different radiative cooling processes (section 2.4) active in both components of the accretion disc and their contributions are shown in Fig. 1. Here, $\nu$ is the frequency of radiation and $L_\nu$ is the emitted luminosity per frequency. We fix a typical values of flow parameters $\mathcal{E} = 1.005$, $\lambda = 2.96$ and $a = 0.6$ to generate the transonic solution and this produces a shock at $x_s = 62.7$. We produce the radiation spectra for SKD mass accretion rate $\dot{m}_h = 0.3$ and that of KD, $\dot{m}_d = 0.5$. We separately present the contributions from the pre-shock region (PRSR) and post-shock region (POSR) of SKD. As mentioned before, we assume that the Keplerian disc truncates at the shock location (Giri & Chakrabarti 2013) and hence POSR contains only sub-Keplerian matter. The pre-shock contributions are synchrotron emission (short-dash magenta line) from the SKD and multi-colour black body contribution (green dot-dash line) from KD. Comptonization of synchrotron soft photons from the PRSR is negligible as PRSR is optically thin. The electron energy distribution in the POSR is hybrid with ∼(10–15)% electrons following a power-law distribution due to acceleration across the shock and rest are thermal electrons. The maximum energy of the accelerated electrons is calculated from the probability of crossing the shock front and the fractional energy gain per crossing (Mandal & Chakrabarti 2005). The synchrotron contribution from POSR is represented by the blue dotted line whereas synchrotron self-Comptonization is shown by the red long-dashed line. Finally, the Comptonization of soft photons from KD by the hot electrons in POSR is represented by orange short-long-dashed line and the overall spectrum is denoted by solid black line. The contribution from bremsstrahlung is insignificant when compared with synchrotron for a stellar mass BH. Hence, we did not show bremsstrahlung spectrum in Fig. 1 to avoid the figure being overcrowded. All these contributions have their individual signature in the spectra. In the figure, the first bump ($\sim 5 \times 10^{15}$ Hz) is the pre-shock synchrotron contribution, the second bump ($\sim 10^{17}$ Hz) is due to KD multi-colour black body photons, the third bump ($\sim 5 \times 10^{19}$ Hz) is Wien cut-off in Comptonized spectrum due to recoil effects of thermal electrons and the fourth bump ($\sim 10^{21}$ Hz) is the cut-off due to non-thermal electrons. It is important to identify these spectral features in the observed spectra as they provide a direct measurement of the system parameters from the observations. For example, the first bump provides the average temperature of the PRSR, the second bump is associated with the KD temperature, the third bump is an indicative of POSR electron temperature and the fourth one is a measure of energy of the accelerated electrons. The second bump is a characteristic signature of the presence of KD, usually observed for BH candidates in soft states whereas the recoil effect (third bump) is observed in the hard state. Also the broken power-law signature $\sim 5 \times 10^{20}$ represents that the non-thermal electrons are contributing toward the very high energy. All these features have been observed in systems like Cyg X-1, GRO J1719-24, GRO J4022+3 (McConnell *et al.* 2002; Pottschmidt *et al.* 2003; Ling & Wheaton 2005).

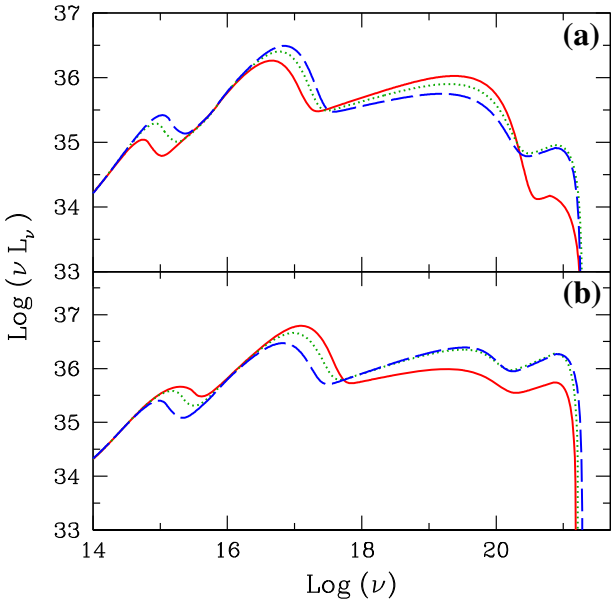


**Figure 2.** Variation of accretion disc radiation spectrum with BH spin parameter. (**a**) The accretion disc is counter-rotating with $a = -0.45$ (solid red), $a = -0.5$ (dotted-green) and $a = -0.55$ (dashed-blue) with the BH. (**b**) The disc is co-rotating with $a = 0.45$ (solid red), $a = 0.5$ (dotted-green) and $a = 0.55$ (dashed-blue) respectively.

In Fig. 2, we present the effect of spin of the BH on the spectral characteristics in the presence of shocks. Transonic shock solutions exist only in a limited range of spin parameter (Sponholz & Molteni 1994; Chakrabarti 1996) for a given value of $(\mathcal{E}, \lambda)$. Hence, we can not compare two solutions with any arbitrary choice of $a$ because those may be completely different solutions. Hence, we fix both $(\mathcal{E}, \lambda)$ and vary the spin parameter $a$ to generate different shock solutions. We present the radiation spectra in two specific situations: in panel (a) accretion disc is counter-rotating ($a$ is negative) with respect to the central BH spin direction and in panel (b) accretion disc is co-rotating ($a$ is positive) along with the central BH. For panel (a) in Fig. 2, we choose $\mathcal{E} = 1.005$ and $\lambda = 3.68$ and the solid-red, dotted-green, dashed-blue spectra are drawn for $a = -0.45$, $-0.5$ and $-0.55$ respectively. Whereas in panel (b), we choose $\mathcal{E} = 1.005$ and $\lambda = 2.96$ and the spectra for different Kerr parameter are shown by solid-red line ($a = 0.45$), green-dotted line ($a = 0.5$), blue-dashed line ($a = 0.55$) respectively. Both the spectra are drawn for the same accretion rate as in Fig. 1. The solution shows that for co-rotating scenario (b), as we increase the Kerr parameter, the location of shock moves outward and the shock strength decreases. The increase in Kerr parameter means increase in effective centrifugal barrier, which always tries to move the shock outward. The shock location is closest to the BH for $a = 0.45$ (red solid line) and hence largest PRSR and smallest POSR. The synchrotron contribution from PRSR as well as black-body photons from KD are the maximum. In this case, the optical depth of POSR is small due to the small size and the average electron temperature of the POSR is smaller in comparison with the other two cases ($a = 0.5$, $a = 0.55$) due to more supply of soft photons from KD. Hence, the contribution towards inverse-Comptonization ($\sim 10^{18}$–$10^{21}$ Hz) of soft photons is also lower. As we increase the spin parameter, the spectral index becomes more harder with increase in hard X-ray luminosity while the low frequency contribution becomes weaker. We see that even if all other parameters are fixed, sources with two different spin parameters show difference in their luminosities and spectral states. A reverse trend occurs for the counter-rotating case, (panel (a)), i.e., the location of shock is moving inward and the shock strength increases as $a$ becomes more and more negative. Consequently, the luminosity in low energy increases while the same in high energy decreases as $a$ becomes more negative.

As we have mentioned earlier, we cannot increase the spin parameter too much since there will be no transonic shock solution for these sets of parameters and hence restrict ourselves to a small range of spin parameter. For higher value of Kerr parameters (say $a = 0.8$), one needs to have different values of input parameters to get a shock solution. A spectral comparison between Fig. 2(a) and (b) shows that for a pro-grade system (Fig. 2(b)), black-body component is more luminous with a softer spectral index than a retrograde system (Fig. 2(a)). Using observed data of several BH sources, Zhang *et al.* (1997) pointed out similar results.

The inverse-Comptonized spectrum shows a power-law ($L_\nu \propto \nu^{-\alpha}$) behaviour and the energy spectral index ($\alpha$) is a measure of hardness ($\alpha < 1.5$ for hard state and for soft state $\alpha > 1.5$) of the emitted radiation. We want to study the effect of Kerr parameter and accretion rate on the spectral index. The spectral index depends on both size (optical depth) and temperature of the Comptonized region (Rybicki & Lightman 1979; Sunyaev & Titarchuk 1980). If both are varied simultaneously, no comparison can be made. Hence, we fix the flow energy $\mathcal{E} = 1.005$, $\dot{m}_h = 0.3$ and change $\lambda$ such that we get shock solution at the same place (constant POSR: $x_s = 21.3$) for three different values of $a$. Then we keep the solution for a fixed $a$ and change $\dot{m}_d$ (which changes the supply of soft black-body photons) to see the changes in $\alpha$. One such study is presented in Fig. 3. Here, the solid-red, dotted-magenta and dashed-blue lines represent the variation of spectral

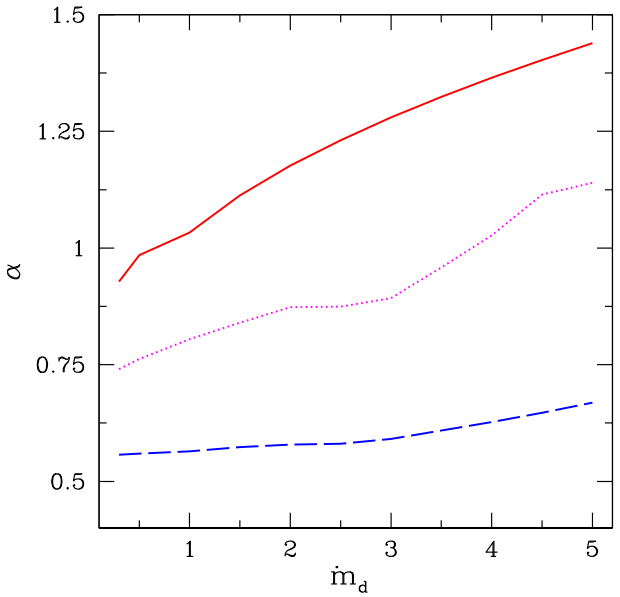


**Figure 3.** Variation of energy spectral index ($\alpha$) with KD accretion rate $\dot{m}_d$ for different Kerr parameters: $a = -0.7$ (solid-red curve), $a = 0$ (dotted-magenta curve) and $a = 0.7$ (dash-blue line). See text for details.

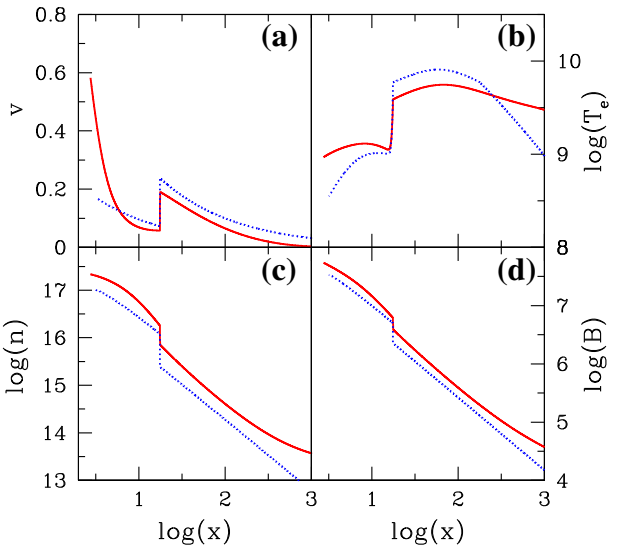


**Figure 4.** Variation of flow parameters in a free-fall parametric solution (blue-dotted line) and transonic shock solution (red-solid line) for $a = 0$. Other parameters are: $\mathcal{E} = 1.005$, $\lambda = 3.3$, $\dot{m}_h = 0.3$ and $\dot{m}_d = 0.5$. We plot the radial velocity in (**a**), electron temperature in (**b**), number density in (**c**) and magnetic field in (**d**). The sharp change in the flow variables shows the shock transition.

index for different combinations ($a = -0.7$, $\lambda = 3.7$), ($a = 0.0$, $\lambda = 3.361$) and ($a = 0.7$, $\lambda = 2.76$) respectively. The figure shows that the radiation spectrum becomes softer (higher $\alpha$; solid-red curve) if the disc is counter rotating ($a = -0.7$) while the spectrum is generally hard (blue-dash curve) in case of co-rotating ($a = 0.7$) disc. Also, we see that as the KD accretion rate increases the spectrum becomes softer as supply of soft black-body photons increases which can cool the hot electrons in POSR more efficiently. A similar result has been reported by You *et al.* (2012) as well.

Chakrabarti and Mandal (2006) studied the radiation properties of an accretion disc around a Schwarzschild BH using the same cooling processes considered here. But that was a parametric study, i.e., instead of taking ($\mathcal{E}$, $\lambda$) as input parameters and getting a transonic solution for both shock location ($x_s$) and compression ratio ($R$), they considered the later two as free input parameters. Hence, whether a combination of ($x_s$, $R$) can be produced from any realistic choice of ($\mathcal{E}$, $\lambda$) was unjustified. Also, they considered a free-fall flow velocity and density distribution. Here, we would like to make a comparison between the variation of the flow parameters from parametric study and transonic solution for the same set of input parameters. This is presented in Fig. 4, where blue-dotted line and red-solid line represent the parameters for free-fall study and transonic shock solution respectively for $a = 0$. The flow parameters are $\mathcal{E} = 1.005$, $\lambda = 3.3$, $\dot{m}_h = 0.3$ and $\dot{m}_d = 0.5$

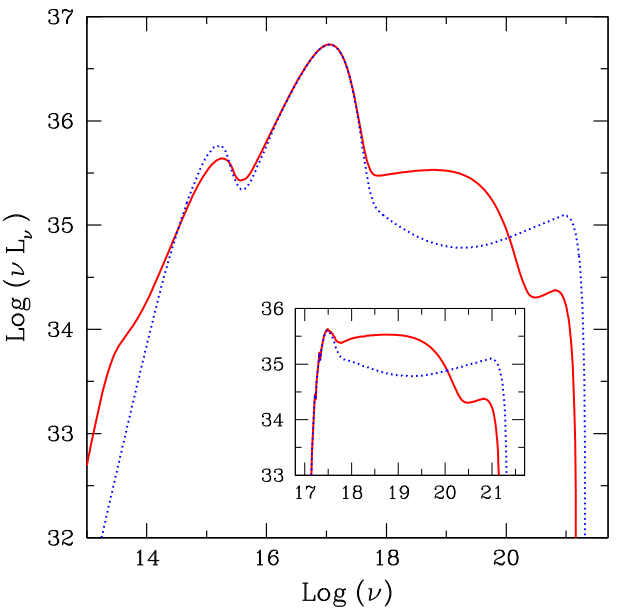


**Figure 5.** Comparison of radiation spectrum using a free-fall parametric solution (blue-dotted line) and transonic shock solution (red-solid line) for $a = 0$. Other parameters are: $\mathcal{E} = 1.005$, $\lambda = 3.3$, $\dot{m}_h = 0.3$ and $\dot{m}_d = 0.5$. The figure in the inset shows the interstellar absorption corrected radiation spectrum.

and this produces a shock at $x_s = 17.6$ with compression ratio $R = 3.28$. We have used the same value of $x_s$ and $R$ for the free-fall case as well. In this figure,

(a) represents the variation of radial velocity, (b) shows the variation in electron temperature, (c) represents the change in number density and (d) corresponds to the variation of magnetic field. The sharp jump represents the shock transition. The corresponding radiation spectra are plotted in Fig. 5 with the same line style as in Fig. 4 and for the same set of input parameters. We clearly see that the red-solid curve differs significantly from the blue-dotted line in the high energy region of the spectrum. A free-fall flow will have large radial velocity (Fig. 4(a)) and hence the flow has less density (Fig. 4(c)) for a given mass accretion rate and hence the free-fall flow is radiatively less efficient. A transonic flow starts with very low radial velocity and the flow spends more time in the outer part of the disc. Hence, an enhanced contribution ($\sim 10^{13}$ Hz in Fig. 5 with red-solid line) from the outer part of the disc. Also a transonic flow has more density and temperature (Fig. 4(b)) in the POSR region. This leads to a harder spectral index with more high energy inverse-Compton contribution ($\sim 10^{19}$ Hz in Fig. 5 with red-solid curve) from thermal electrons. The high energy contribution from non-thermal electrons do not depend on temperature. A free-fall flow has less optical depth and hence a higher escape probability of photons from POSR. That is why non-thermal electron Comptonization is relatively higher ($\sim 10^{21}$ Hz in Fig. 5 with blue-dashed line) in a free-fall flow.

Is it possible to identify all these spectral properties (different bumps, spectral indices, exponential cut-off) in the observed spectrum? To answer this, we have convolved these radiation spectrum with the interstellar absorption model (Rumph *et al.* 1994; Morrison & McCammon 1983). We assume a typical interstellar hydrogen column density $n_{\rm H} \sim 10^{22}$ atoms cm$^{-2}$. The result is presented in the inset of Fig. 5. We see that all the spectral features below $10^{17}$ Hz are washed out due to interstellar absorption and hence probing the PRSR contributions in the observed spectrum are not feasible. But the high energy features are all present and can be identified in the observed spectrum.

## 4. Summary

We study the radiation spectral properties around a rotating BH. We have included the effect of heating/cooling in the transonic solutions by adopting an iterative method and use these solutions to calculate the radiation spectrum. In Fig. 1, we have shown different contributions of cooling processes in the spectra. We see that synchrotron and multi-colour black-body photons are the most dominant sources of soft photons and inverse Comptonization of these soft photons dominates the high energy X-ray spectrum. A GRMHD simulation of accretion disc by McKinney *et al.* (2017) has shown similar results in the presence of double Compton and synchrotron radiation with much larger accretion rate. Also, we see that the very high energy part of the spectrum is contributed by non-thermal electrons with a spectral break from thermal electrons. Figure 2 shows the effect of spin parameter in the spectrum. In a pro-grade scenario, as $a$ increases, the spectrum becomes harder with more high energy luminosity and the low energy contribution decreases whereas in the retrograde case, we see just the reverse trend. The energy spectral index also depends on $a$. The higher efficiency of energy production in pro-grade scenario is generally expected and has been shown through extensive numerical simulations (Narayan *et al.* 2017). In Fig. 3, we present variation of spectral index ($\alpha$) with the KD accretion rate for three different values of $a$. Since spectral index depends on both optical depth and average temperature of POSR, we choose the input parameters such that they produce the same size of POSR. The spectral index becomes harder as $a$ changes from a negative value to a positive value. Also $\alpha$ increases with increase in $\dot{m}_d$, as this increases the soft photon supply. Finally, in Fig. 5, we compare the radiation spectrum from a free-fall solution and a transonic solution. We see significant differences in high energy contribution from the two solutions. A transonic solution provides more hotter and denser POSR and hence an enhanced high energy contribution.

Finally, this kind of study will be helpful to understand the observed broadband radiation spectrum of the reportedly highly spinning BH candidates like GRS 1915+105, GRO J1655-40 (Zhang *et al.* 1997; Orosz & Bailyan 1997; Remillard *et al.* 1997). In future, we plan to include all the general relativistic effects (redshift, photon bending and focusing, etc.) in our spectral calculations and we wish to compare our model spectra with observed broadband energy data.

## References

Abramowicz M. A. *et al.* 1995, ApJ, 452, 379
Artemova I. V., Bjoernsson G., Novikov I. D. 1996, ApJ, 461, 565
Bao, G., Hadrava, P., Ostgaard, E. 1994, ApJ, 425, 63
Bell A. R. 1978a, MNRAS, 182, 147
Bell A. R. 1978b, MNRAS, 182, 443
Belloni T., Méndez M., Sánchez-Fernández C. 2001, A&A, 372, 551

Belloni T., Homan J., Casella P. *et al.* 2005, A&A, 440, 207
Bondi H. 1952, MNRAS, 112, 195
Chakrabarti S. K. 1989, ApJ, 347, 365
Chakrabarti S. K. 1990, Theory of Transonic Astrophysical Flows, World Scientific, Singapore, Volume 150
Chakrabarti S. K. 1996, MNRAS, 283, 325
Chakrabarti S. K., Khanna R. 1992, MNRAS, 256, 30
Chakrabarti S. K., Titarchuk L. G. 1995, ApJ, 455, 623
Chakrabarti S. K., Mandal S. 2006, ApJL, 642, L49
Chakrabarti S. K., Mondal S. 2006, MNRAS, 369, 976
Chattopadhyay I., Chakrabarti S. K. 2002, MNRAS, 333, 454
Colpi M., Maraschi L., Treves A. 1984, ApJ, 280, 319
Cunningham C. T. 1975, ApJ, 202, 788
Das S. 2007, MNRAS, 376, 1659
Dermer C. D., Liang E. P., Canfield E. 1991, ApJ, 369, 410
Ebisawa K., Mitsuda K. 1991, ApJ, 367, 213
Fragile P. C., Blaes O. M., Anninos P., Salmonson J. D. 2007, ApJ, 668, 417
Fukue J. 1987, PASJ, 39, 309
Galeev A. A., Rosner R., Vaiana G. S. 1979, ApJ, 229, 318
Giri K., Chakrabarti S. K. 2013, MNRAS, 430, 2836
Hanawa T. 1989, ApJ, 341, 948
Hawley J. F., Villiers J. D. 2004, PThPS, 155, 132
Ichimaru S. 1977, ApJ, 214, 840
Ivanov R. I., Prodanov E. M. 2005, Phys. Lett. B, 611, 34
Iyer N., Nandi A., Mandal S. 2015, ApJ, 807, 108
Jorstad S. G., Marscher Alan P. 2004, ApJ, 614, 615
Li L. et al. 2005, ApJS, 157, 335
Ling J. C., Wheaton W. A. 2005, Astron. Astrophys., 5, 80
Lightman A. P., Eardley D. M. 1974, ApJ, 187, L1
Luminet J. P. 1979, A&A, 75, 228
McConnell M. L. *et al.* 2002, ApJ, 572, 984
McKinney J. C., Chluba J., Wielgus M. *et al.* 2017, MNRAS, 467, 2241
Mandal S., Chakrabarti S. K. 2005, A&A, 434, 839
Matsumoto R., Kato S., Fukue J., Okazaki A. T. 1984, PASJ, 36, 71
Mirabel I. F., Rodríguez L. F. 1999, ARA&A, 37, 409
Mondal S., Chakrabarti S. K. 2006, MNRAS, 371, 1418
Morrison R., McCammon D. 1983, ApJ, 270, 119
Muchotrzeb B., Paczyński B. 1982, Acta Astron., 32, 1
Mukhopadhyay B. 2002, ApJ, 581, 427
Nandi A., Debnath D., Mandal S., Chakrabarti S. K. 2012, A&A, 542, 56
Narayan R., Yi I. 1995, ApJ, 452, 710
Narayan R., Sądowski A., Soria R. 2017, MNRAS, 469, 2997
Novikov I. D., Thorne K. S. 1973, in Dewitt C., Dewitt B., eds, Black Holes, Gordon & Breach, New York, Volume 343.
Orosz J. A., Bailyan C. D. 1997, AJ, 477, 876
Paczyński B., Wiita P. J. 1980, A&A, 88, 23
Page D. N., Thorne K. S. 1974, ApJ, 191, 499
Patrick A. R., Reeves J. N., Porquet D. *et al.* 2012, MNRAS, 426, 2522
Pottschmidt K. *et al.* 2003, A&A, 411, 383
Rees M. J., Begelman M. C., Blandford R. D., Phinney E. S. 1982, Nature, 295, 17
Reeves J. N., Fabian A. C., Kataoka J. *et al.* 2006, Astron. Nachr., 327, 1079
Remillard R. A. *et al.* 1997, in Olinto A., Frieman J., Schramm D., eds, Proceedings of the 18th Texas Symposium on Relativistic Astrophysics, University of Chicago
Remillard R. A., McClintock J. E. 2006, ARA&A, 44, 49
Rybicki G. B., Lightman A. P. 1979, Radiative Processes in Astrophysics, Wiley, New York
Rumph T., Bowye S., Vennes S. 1994, ApJ, 101, 2108
Sabatini S., Tavani M., Coppi P. *et al.* 2013, ApJ, 766, 83
Sądowski A., Narayan R., McKinney J. C. *et al.* 2014, MNRAS, 439, 503
Sądowski A., Narayan R., Tchekhovskoy A. *et al.* 2015, MNRAS, 447, 49S
Sądowski A., Wielgus M., Narayan R. *et al.* 2017, MNRAS, 466, 705
Semerák O., Karas V. 1999, A&A, 343, 325
Shakura N. I., Sunyaev R. 1973, A&A, 24, 337
Smith D., Heindl W. A., Markwardt J. H., Swank, J. H. 2001, ApJ, 554, L41
Smith D. M., Heindl W. A., Swank J. H. 2002, ApJ, 569, 362
Sponholz H., Molteni D. 1994, MNRAS, 271, 233
Sun W. H., Malkan M. A. 1989, ApJ, 346, 68
Sunyaev R. A., Titarchuk L. G. 1980, A&A, 86, 121
Sunyaev R. A., Titarchuk L. G. 1985, A&A, 143, 374
Strohmayer T. E. 2001, A&A, 554, L169
You B., Cao X., Yuan Y. 2012, ApJ, 761, 10
Zhang S. N., Cui W., Chen W. 1997, ApJ, 482, L155
Zeldovich Y. B., Raizer Y. P. 1968, Elements of Gas Dynamics and the Classical Theory of Shock Waves, Academic Press, New York